DOI:
10.1016/j.msec.2019.110620

Document Version
Peer reviewed version

Surface Engineered Nanoliposomal Platform for Selective Lymphatic Uptake of Asenapine Maleate: *In vitro* and *In vivo* Studies

Renuka S. Managuli[a], Julie Tzu-Wen Wang[b], Farid Muhammad Faruqu[b], Abhjieet Pandey[a], Sanyog Jain[c], Khuloud T Al-Jamal[b], Srinivas Mutalik[a,*]

[a] Department of Pharmaceutics, Manipal College of Pharmaceutical Sciences, Manipal Academy of Higher Education, Manipal 576104, Karnataka State, India

[b] School of Cancer and Pharmaceutical Sciences, King's College London, Franklin-Wilkins Building, 150 Stamford Street, London SE1 9NH, UK

[c] Centre for Pharmaceutical Nanotechnology, Department of Pharmaceutics, National Institute of Pharmaceutical Education and Research, Sector 67, S.A.S. Nagar (Mohali), Punjab 160062, India

*** For correspondence:**

Dr. Srinivas Mutalik

Department of Pharmaceutics

Manipal College of Pharmaceutical Sciences

Manipal Academy of Higher Education, Manipal 576104

Karnataka State, India

Email: ss.mutalik@manipal.edu

Phone: +91-820-2922482

Abstract

Asenapine maleate (ASPM) is an antipsychotic drug prescribed for the treatment of schizophrenia and bipolar disorder. ASPM possesses low oral bioavailability due to extensive hepatic metabolism. Therefore, RGD peptide conjugated liposomes loaded with ASPM were prepared to target Peyer's patches in the intestine which in-turn get access into intestinal lymphatic system thereby increasing the oral bioavailability of the drug. Liposomes were evaluated for size, zeta potential, differential scanning calorimetry (DSC), FTIR spectroscopy, X-ray diffraction (XRD), shape and morphology, *in vitro* drug release, cell line studies, everted intestinal uptake, pharmacodynamics, pharmacokinetics, tissue distribution, targetability and stability studies. *In vitro* drug release study showed the sustained release of drug from the formulations. Optimized liposomes (size < 110 nm) showed greater permeability across the Caco2+Raji B co-culture model *in vitro* and everted rat ileum *ex vivo*. Liposomes showed increase in bioavailability and high efficacy in reducing the L-DOPA-carbidopa induced locomotor count compared to plain drug. Liposomes also showed high concentration of drug in the brain after their oral administration. Imaging studies showed that RGD peptide conjugated liposomes were successful in targeting the Peyer's patches, both *in vivo* and *ex vivo*. The study successfully demonstrated the improved pharmacokinetics and efficacy profile of ASPM by using a ligand conjugated targeted liposomal system.

Keywords: Asenapine maleate; RGD peptide; Peyer's patches; liposomes

1. Introduction

For drugs undergoing extensive first pass metabolism, drug delivery toward intestinal lymphatic system (ILS) is an attractive pathway. Since ILS transports molecules directly into systemic circulation, drug metabolism in the liver can be overcome, resulting in improved oral bioavailability (Managuli et al., 2018). Asenapine maleate (ASPM) is an antipsychotic drug used for schizophrenia and bipolar 1 disorder treatment. It is available in the market as sublingual tablets since its oral bioavailability is low due to first pass metabolism. The drawbacks of sublingual tablets are the inconvenience of holding the dose in the mouth, tongue numbness and drug loss if swallowed. Patients' noncompliance to the sublingual tablets is a major problem in the treatment of mental illness because antipsychotics need to be taken for a longer period and it is difficult to expect psychiatric patients to administer sublingual tablets via the suggested route. Moreover, the schizophrenic patients are generally prescribed with more than one kind of medications. If the dosage form of a different route of administration (e.g., sublingual tablet in case of ASPM) is prescribed along with an orally administered dosage form, then it is most likely that the patients get confused and they may consume all the medications orally leading to drug abuse.

With this regard, there have been many studies developing ASPM in various formulations for different administration routes including nanostructured lipid carriers for oral lymphatic uptake (Managuli et al., 2019), solid lipid nanoparticles for oral delivery (Patel et al., 2019), sublingual film (Kapadia et al., 2013), thermo-responsive in situ nasal gel (Kulkarni and Avachat, 2017), nanostructured lipid carriers for intranasal delivery (Singh et al., 2016) and three patents are available on intranasal (Patent US20080306133A1), transdermal (Patent WO2010127674A1) and injectable (Patent WO2010149727 A3) formulations of asenapine. The ease and convenience of the oral route in the treatment of psychic disorders are greatly appreciated among patients and healthcare professionals. To overcome the challenge of the first pass metabolism of ASPM in an oral dosage form, we recently developed ASPM loaded nanostructure lipid carriers (NLCs) to improve the oral bioavailability as NLCs can be taken up into lacteal of intestinal villi in the form of chylomicrons because of the lipidic nature of the carrier (Managuli et al., 2019). Molecular access to ILS can be achieved either via lacteal villi of the intestine or through Peyer's patches. Peyer's patches are lymphoid aggregates which are present in the intestine. These patches are enclosed by follicle-associated epithelium (FAE), which acts as the interface across the luminal environment and the gut-associated lymphoid tissue (GALT) (Jung et al., 2010). The FAE comprised of specialized cells called as M cells (for microfold) which have high transcytotic activity (Mabbott et al., 2013). M cells of Peyer's patches are overexpressed with β1 integrins at their apical surface (Clark et al., 1998; Miller et al., 2007). β1-Integrins can be targeted by various ligands like Arginine-Glycine-Aspartic acid (RGD) peptide (Fievez et al., 2009; Yun et al., 2013).

In the present work, RGD peptide conjugated liposomes were prepared to enhance the selective lymphatic uptake through Peyer's patches. The prepared liposomes were extensively characterized using various techniques such as differential scanning calorimeter (DSC), Fourier Transform Infrared (FTIR) spectroscopy, X-ray diffraction (XRD) studies, transmission electron microscopy (TEM), drug release studies, particle size etc., to name a few along with multiple in vitro including cell line studies. Ex vivo and in vivo studies including everted intestinal uptake, pharmacodynamics, pharmacokinetics, tissue distribution and assessment of targetability were performed.

2. Materials and Methods

2.1. Materials

ASPM was obtained from MSN Organic Pvt. Ltd. (Hyderabad, India) and Orbicular Pharm Tech R&D (Hyderabad, India) as a gift sample. 1,2-distearoyl-sn-glycero-3-phosphocholine (DSPC), 1,2-distearoyl-sn-glycero-3-phosphoethanolamine-N-diethylenetriaminepentaacetic acid (ammonium salt) (DSPE-DTPA) and linker DSPE-PEG_{2000}-Maleimide were obtained from Avanti Polar Lipids, Inc. (Alabama, USA). RGD peptide, 1′-Dioctadecyl-3,3,3′,3′-tetramethylindocarbocyanine perchlorate (DiI), N-(3-Dimethylaminopropyl)-N′-ethylcarbodiimide hydrochloride (EDC. HCl), Fluorescein 5-isothiocyanate (FITC) and N-Hydroxysuccinimide (NHS) were obtained from Sigma Aldrich (MO, USA). Arginine-Glycine-Aspartic acid-Cysteine trifluoroacetate salt (RGDC) was purchased from Bachem Distribution Services (GmbH, Germany). Linker 1,2-distearoyl-sn-glycero-3-phosphoethanolamine-N-[carboxy(polyethylene glycol)-2000] (ammonium salt) (DSPE-PEG_{2000}-COOH) was obtained from Nanocs Inc. (NY, USA). Indium-111 was obtained from Mallinckrodt (Netherland). Sepharose CL-2B was purchased from GE Healthcare Bio-Sciences (AB, Sweden). Indium-111 chloride was obtained from Mallinckrodt (Netherlands). 1,2-distearoyl-sn-glycero-3-phosphoethanolamine-N-diethylenetriaminepentaacetic acid (ammonium salt) (DSPE-DTPA) was purchased from Avanti Polar Lipids, Inc (USA). Thin layer chromatography (TLC) strips for radiolabelling were purchased from Agilent Technologies UK Ltd. (Wokingham, UK). NAP-5 desalting columns were obtained from GE Healthcare Life Sciences (UK).

2.2. Preformulation studies

Drug-excipients compatibility was assessed by FTIR spectroscopy and DSC. Plain ASPM and its physical mixture with lipids (DSPC and cholesterol) were subjected to FTIR and DSC.

2.3. Preparation of liposomes

ASPM loaded liposomes were prepared by thin film hydration technique using DSPC and cholesterol. The solution of ASPM, lipid, and cholesterol made in chloroform was poured in a round bottom flask and subjected to evaporation under vacuum in Rotavapor (R-215, Buchi Labortechnik

AG, Flawil, Switzerland) at 60 °C and 120 rpm. The thin lipid film formed around the wall of the flask was hydrated with phosphate buffer of pH 7.4 and the obtained coarse liposomal dispersion was probe sonicated (Probe sonicator VC 130, Sonica and Material Inc, USA) to reduce the particle size. Formulation optimization was carried out by changing the ratios between different compositions and sonication duration (Table *S1*).

2.3.1. Preparation of conjugated liposomes

Optimized liposomes containing DSPC and cholesterol in the molar ratio of 1:0.5 (LP-3) was selected for RGD conjugation. DSPE-PEG_{2000}-COOH and DSPE-PEG_{2000}-maleimide were used as a linker for RGD and RGDC conjugation, by EDC-NHS and maleimide-thiol reaction, respectively. Linkers were added during the thin film formation step in the preparation of liposomes at the molar ratio of 2:0.02 of DSPC and linker. RGD conjugated liposomes were prepared by following method. Covalent binding of RGD to carboxyl functionalized liposomes (LP-COOH) comprising DSPC, cholesterol, and DSPE-PEG_{2000}-COOH (2:1:0.02 molar ratio, a total lipid of 29.8 mM) using EDC-NHS chemistry. The carboxyl-functionalized liposomes (0.2 mM linker), EDC (200 mM) and NHS (200 mM) were added and incubated for 1 h at room temperature. After 1 h, RGD (1:2 linker: RGD molar ratio; RGD: 0.4 mM) was added and the reaction mixture was gently stirred overnight at 4 °C for conjugation to accomplish. Any excess amount of added reactants was separated by dialysis against MES buffer at pH 5.5 using dialysis membrane (MWCO 12 kDa). This resulted in the formation of RGD functionalised LP-COOH (LP-CONH-RGD).

Along with above, other set of liposomes (LP-MAL-RGD) was prepared which was only used in SPECT and optical imaging studies. In this approach, covalent binding of RGDC to maleimide functionalized liposomes (LP-MAL) comprising DSPC, cholesterol, and DSPE-PEG_{2000}-maleimide (2:1:0.02 molar ratio, a total lipid of 29.8 mM) was achieved by maleimide-thiol "click" chemistry. The maleimide functionalized liposomes, RGDC (1:2 linker: RGDC molar ratio; RGDC: 0.4 mM) was added and was incubated at 4 °C overnight. Excess RGDC was separated using a Sepharose CL-2B column. This resulted in the formation of RGD functionalised LP-MAL-RGD. Quantification of lipid was done using standard Stuart assay (SI). The composition of conjugated liposomes is given in Table *S2*.

2.4. DSC, FTIR and X-Ray Diffraction (XRD) studies

To assess any change in crystalline nature of drug when encapsulated in liposomes, plain drug and optimized liposomal formulation (lyophilized with 5% w/v sucrose) were subjected to XRD, FTIR and DSC studies. FTIR analysis was also performed for the linker DSPE-PEG_{2000}-COOH, RGD conjugated linker (DSPE-PEG_{2000}-RGD), and carboxyl functionalized liposomes to confirm the formation of amide bond after conjugation.

2.5. Particle size, PDI, zeta potential and determination of particle concentration

The average particle size, PDI and zeta potential of the liposomes were determined by Malvern Zetasizer (Nano ZS, Malvern Instruments, UK). Similarly, the liposomes were assessed for stability at storage condition of 5 ± 3 °C and 25 ± 2 °C/60 ± 5% relative humidity (RH) for 6 months. The stability samples were analysed after 7 days, 15 days, 1, 3 and 6 months for size, PDI, zeta potential and entrapment efficiency. The particle concentration in the optimized liposomal dispersions was measured by using NanoSight (Malvern Instruments, UK).

2.6. Entrapment efficiency

Drug entrapment efficiency was determined by lysing the liposomes and then estimating the drug content using HPLC. Any un-entrapped drug in liposomal dispersion was removed from entrapped particles by centrifugation at 22,000 rpm and 4°C for 30 min. The separated supernatant was further centrifuged at same condition and the pellet obtained in both the steps was ruptured with 1% w/v Triton X-100 solution. The resultant solution was diluted with the mobile phase buffer and filtered through a 0.22 µm membrane. The samples were quantified by using HPLC (LC2010CHT, Shimadzu Corporation, Japan). The chromatographic conditions involved the use of phosphate buffer containing 0.1%v/v TEA (pH adjusted to 3.0 ± 0.05 with dilute ortho-phosphoric acid) and ACN mixture in the ratio of 80:20% v/v as mobile phase and Hyperclone BDS C18 column (250 × 4.6 mm, 5 ??m) as stationary phase. The mobile phase was pumped at a flow rate of 1.0 mL/min and the eluent was detected at the wavelength of 230 nm. Both column and auto-sampler temperature was maintained at 25 °C and injection volume was set to 20 ??L with a run time of 11 min. Entrapment efficiency was calculated using the formula.

$$\text{Entrapment efficiency (\%)} = \frac{[ASPM]_E}{[ASPM]_T} \times 100$$

where, $[ASPM]_E$ corresponds to the amount of entrapped drug and $[ASPM]_T$ represents the total amount of ASPM in nanoformulation.

2.7. Transmission electron microscopy

Shape and surface morphology of the unconjugated liposomes (LP-3) and RGD conjugated liposomes (LP-CONH-RGD) were studied using transmission electron microscope (CM200 supertwin System, Netherland). A sample drop was placed on a carbon coated copper grid and air dried. Excess sample was removed from corner by using filter paper. Phosphotungstic acid solution (1% w/v, pH 6.0) was added to stain the sample and dried under IR lamp.

2.8. In vitro drug release study

In vitro release of ASPM from liposomes was performed in hydrochloric acid (HCl) solution of pH 1.2 for 2 h, ammonium acetate buffer of pH 4.5 for 1 h, pH 6.8 phosphate buffer for 6 h and

pH 7.4 phosphate buffer for 48 h by dialysis method (Li et al., 2010; Shete and Patravale, 2013). The liposomal dispersion (equivalent to 2 mg drug) was transferred in a dialysis bag (MWCO: 12,000 Da) which was suspended in 100 mL of each media, kept on a magnetic stirrer with speed 100 rpm at 37 ± 0.5 ºC. Aliquots of 2 mL were withdrawn and replaced the same volume with fresh media. The withdrawn sample was analyzed for drug release using HPLC.

2.9. Cell uptake study

Cells uptake in human colon cancer Caco-2 cell monoculture and in a co-culture model consisting Caco-2 cells and human B lymphocytes Raji B cells was performed in a Corning® Costar® 6-well flat bottom culture plates. The cells at a density of 5×10^5 per well were incubated overnight in HBSS medium at 37 ℃ in 5/95 (%v/v) CO_2/air atmosphere. The medium was replaced with the fresh serum-free medium after 24 h of incubation. The cells were treated with free FITC and FITC-labeled liposomes (LP-3 and LP-CONH-RGD) at the concentration of 10 µg/mL (S2). The medium was discarded after 2 h of the incubation period and the cells were washed three times with cold PBS. Trypsin (0.05%)/EDTA (0.02%) solution was added to detach the cells and further washed with cold PBS. The cells were centrifuged at 4000 rpm and the supernatant was discarded. The cells were re-suspended in 1 mL of PBS and the uptake efficiency was determined using a confocal laser scanning microscope (FV 1000 SPD Olympus, USA).

2.10. Cell permeability study

Cell permeability study was conducted on a Caco-2 monoculture and in the Caco-2 and Raji B co-culture model developed onto Transwell® polycarbonate inserts (pore diameter 3 µm) in 12 well plates. Monolayers with TEER values (Millicell-ERS, Millipore Corporation, Germany)) above 400 Ω were selected for the experiment. The apical side of the monolayer was supplied with 0.5 mL and the basolateral side was supplied with 1.5 mL volume of culture medium. The medium was replaced 5 days after seeding and thereafter every 2 days. The integrity of the monolayer was determined by measurement of TEER as well as lucifer yellow transport at the end of each experiment. ASPM solution, LP-3 liposomes and LP-CONH-RGD contained in 0.5 mL HBSS (pH 7.4) and 1.5 mL of HBSS (pH 7.4) were added to the apical and basolateral chambers, respectively. Drug transport study was performed from the apical side to the basolateral side. The amount of ASPM transported in the basolateral side was determined by HPLC (Derakhshandeh et al., 2011). The apparent permeability or permeability coefficient (P*app*) was calculated by using following formula.

$$\mathrm{P}app = \left(\frac{\mathrm{dQ}}{\mathrm{dt}}\right) \mathrm{x}\ 1/\mathrm{AC}$$

where, dQ/dt corresponds to the slope of the cumulative concentration of the drug in receptor medium over time; A corresponds to surface area and C corresponds to initial drug concentration in donor chamber.

2.11. Cell toxicity by MTT assay

MTT assay was performed on Caco-2 monoculture as well as Caco-2 and Raji B for plain drug solution, LP-3 liposomes and LP-CONH-RGD liposomes. About 5000 cells/well was seeded in 96-well plates. The cells were grown in 5/95 (% v/v) CO_2/air atmosphere for 24 h at 37 ºC with the supplementation of DMEM medium (100 µL) provided with 1% (v/v) penicillin-streptomycin. The adhered cells were then treated with plain drug solution, LP-3 liposomes, and LP-CONH-RGD at various concentration ranges (1-20 µM/mL) for 48 h at 37 °C. The treated medium was discarded, and cells were washed with fresh culture media. Later, in each well 50 µL of freshly prepared MTT reagent (2 mg/mL) in phosphate buffer saline (PBS) was added. The plate was shaken and incubated for 3 h at 37 ºC in 5/95 (% v/v) CO_2/air atmosphere. After incubation, the supernatant layer was discarded from each well. Later, the formazan crystals formed in the cells were solubilized by addition of iso-propanol (50 µL). The absorbance of formazan solution in iso-propanol was determined by using a Micro-plate reader at a wavelength of 540 nm.

2.12. Animal studies

Ex vivo and *in vivo* studies were performed on in-bred male Sprague-Dawley rats (200–250 g) at (1) Central Animal Research Facility, Manipal Academy of Higher Education, India; (2) School of Cancer and Pharmaceutical Sciences, King's College London, UK. The study protocol was approved by the Institutional Animal Ethical Committee, Kasturba Medical College, Manipal (Approval No: IAEC/KMC/42/2014). For the work conducted in the UK, animal experiments were performed in compliance with the UK Home Office (1989) Code of Practice for the housing and care of Animals used in Scientific Procedures.

2.12.1. Ex vivo everted ileum sac technique

Overnight fasted rats were sacrificed humanely, and the small intestine was isolated. The ileum part (≈ 8 cm) was carefully everted by using the glass capillary and tied between the cannulated cut of the 'U' shaped perfusion apparatus. The perfusion apparatus was kept in a flask containing Ringer's solution of pH7.4 (450 mL). The medium was stirred by using a magnetic bead at 100 rpm and 37 °C. The ASPM solution/LP-3/ LP-CONH-RGD was incorporated in Ringer's solution. The aliquots were withdrawn from the upper end of the cannulated arm of the 'U' tube at time intervals of 1, 2 and 3 h and the same volume was replaced with fresh Ringer's solution from another arm of 'U' tube. The samples were analyzed for the drug amount by HPLC.

2.12.2. Pharmacokinetic and tissue distribution study

The rats were grouped as: Group I: plain ASPM solution; Group II: LP-3 liposomes; Group III: LP-CONH-RGD. All the groups received ASPM dose of 15.8 mg/Kg body weight per orally. Blood was collected from retro-orbital plexus at different time points between 0 and 72 h in the tubes containing disodium EDTA (n=6). Plasma was separated by centrifugation of blood at 5000 rpm for

10 min and stored at -80 ºC till further use. Pharmacokinetic parameters were assessed by using Phoenix® WinNonlin™ 6.4 software (Certara USA Inc., New Jersey, USA). For tissue distribution study, rats (n=9) were sacrificed at time points of 1, 8 and 24 h to isolate the brain, liver, kidney, spleen and small intestine. The isolated organs were weighed and homogenized with saline (1-3 mL) and 100 µL of TFA under ice bath. The homogenates were centrifuged at 18000 rpm for 10 min at 10 °C and the supernatant obtained was analyzed by using HPLC.

2.12.3. Pharmacodynamics study

The efficacy study involved the use of hyperactivity animal model induced by using psychostimulants like levodopa (L-dopa) and carbidopa. These psychostimulants were injected in rats to increase locomotor activity (LMA). Effect of the optimized formulation in order to reduce the hyperactivity of rats was studied by dividing them into five groups (n=4):

Group I: Negative control group (no treatment); Group II: Positive control group, LMA induced in rats with L-dopa (10 mg/Kg) and carbidopa (2.5 mg/Kg) intraperitoneally; Group III: Group II treated with oral ASPM solution (15.8 mg/Kg); Group IV: Group II treated with oral LP-3 liposomes equivalent to 15.8 mg/Kg of ASPM; Group V: Group II treated with oral LP-CONH-RGD equivalent to 15.8 mg/Kg of ASPM. LMA was examined at 1, 2 and 3 h for 5 min by using digital actophotometer (IKON, India). The LMA of rats in group II was assessed after 1 h of L-dopa-carbidopa administration. In group III, IV and V, ASPM solution/ LP-3/ LP-CONH-RGD were administered after 30 min of L-dopa-carbidopa administration. LMA was examined after 30 min of the treatment.

2.12.4. Assessment of targetability of RGD conjugated liposomes to Peyer's patches by whole-body SPECT/CT imaging and gamma scintigraphy

i. *Radiolabelling of liposomes:* Liposomes (LP-MAL-RGD) were prepared with the incorporation of DSPE-DTPA (1% w/w of total lipid). The radioactive ^{111}In solution (30 MBq) prepared in ammonium acetate buffer (1M, pH 5.5) was added to the liposome-DTPA formulation. This mixture was incubated for 30 min at room temperature for labeling to occur. After labeling with [^{111}In], EDTA was used to chelate free [^{111}In]. The unbound [^{111}In] EDTA was removed by eluting the radiolabeled liposomes though NAP-5 desalting column equilibrated with PBS.
ii. *Radiolabelling efficiency and stability studies:* The radiolabeled liposomal fractions were spotted on glass microfiber chromatography paper strips impregnated with silica gel. These TLC strips were then developed using a mobile phase of 0.1 M ammonium acetate solution of pH 5.6 containing 25 mM EDTA. The developed strips were fixed on multi-purpose storage phosphor screen in an autoradiography cassette (Biomax Cassette®, Kodak, US) for exposure. Quantitative autoradiography counting was then performed using a cyclone phosphor detector (Packard®, Australia). The radiolabelling stability was assessed by incubating radiolabelled samples in PBS

or serum (1:1% v/v) for 24 h at 37 ºC. The percentage of ^{111}In remained conjugated to the liposomes was evaluated by TLC.

iii. *SPECT/CT imaging:* Overnight-fasted rats were orally administered with [^{111}In]LP-MAL and [^{111}In]LP-MAL-RGD (31.3 mg/kg and 30.8 mg/kg, respectively, ~28 MBq, ~1 mL). Rats were imaged with nano-SPECT/CT scanner (Bioscan ®, USA) 0–40 min, 4 h and 24 h post oral administration. The SPECT scans were acquired over 24 projections (60 s per projection), using a 4-head scanner with 1.4 mm pinhole collimators, for a total acquisition time of 30-40 min. CT scans were obtained at the end of each SPECT acquisition using 45 Kvp. All data were reconstructed with MEDISO (Medical Imaging System) and the combining of the SPECT and CT acquisitions were performed using InVivoScope^{TM} software (Bioscan, Washington DC, USA).

iv. Tissue biodistribution studies: [^{111}In]LP-MAL-RGD (164 mg lipid/kg, 11.8 MBq, 1.62 mL) and [^{111}In]LP was administered orally to overnight fasted rats. After 1 h and 3 h of administration, the rats were sacrificed and major organs (brain, lung, liver, intestine, spleen, heart and kidneys) were collected. Gamma radiation from isolated organs placed in scintillation vials was counted by LKB Wallac gamma counter (1282 Compu Gamma CS, PerkinElmer, Massachusetts, USA). One centimeter intestinal segments containing Peyer's patches and their adjacent segments (1 cm) without Peyer's patches (non-Peyer's patches) were harvested and placed in scintillation vials. Peyer's and non-Peyer's patches intestinal segments were analyzed by gamma counting. Results were plotted as percentage of injected dose per organ or per 16 patches.

2.12.5. Ex vivo optical imaging and quantification

Fluorescently labeled liposomes were prepared with the incorporation of DiI dye in the lipid/drug mixture in chloroform (0.5% w/w of total lipid) formulated and purified following the same procedures described previously. For *in vivo* studies, the resulting LP-DiI and LP-MAL-RGD-DiI were administered to overnight fasted rats at a dose of 164 mg lipid/kg rat. After 1 h and 3 h of oral administration, the rat was sacrificed, and intestine was collected. The intestine was washed thoroughly and cut into 1 cm segments containing Peyer's and non-Peyer's patches. These intestinal segments were imaged at excitation/emission λ of 540/570 nm by IVIS *in vivo* optical imaging system (Lumina III, , PerkinElmer, US) and the total radiant efficiency was calculated and plotted against patches of LP-DiI at 1 h (Number of patches, n=29), LP-DiI at 3 h (N= 14), LP-MAL-RGD-DiI at 1 h (N=31) and LP-MAL-RGD-DiI at 3 h (n=12).

Ex vivo studies were performed using the ileum sac isolated from overnight fasted rats. After dissection, the intestine was immediately flushed off with freshly prepared Kreb's-Ringer bicarbonate buffer (pH 7.4). One end of the intestine was tied and the fluorescent labeled formulation (LP-DiI/ LP-MAL-RGD-DiI) was instilled into intestinal lumen from another side. Both ends were securely tied, and the intestine was placed into a beaker containing Kreb's-Ringer bicarbonate buffer

pH 7.4. The whole apparatus was mounted on a magnetic stirrer and the experiment was carried out at 100 rpm and 37 °C with continuous aeration. After 3 h, the intestine was thoroughly washed and the entire ileum and 1 cm segments containing Peyer's and non-Peyer's patches were imaged by IVIS *in vivo* imaging system. Total radiant efficiency was measured and plotted against patches of LP-DiI at 1 h (Number of patches, n=29), LP-DiI at 3 h (n= 14), LP-MAL-RGD-DiI at 1 h (n=31) and LP-MAL-RGD-DiI at 3 h (n=12).

2.13. Statistical analysis

GraphPad Prism 5.03 was used for statistical analysis of data obtained. Unpaired *t*-test at 5% significance level was used to obtain two-tailed *p*-value for two group data and One-way ANOVA followed by Tukey's post hoc test was utilized for more than two group comparison.

RESULTS

3.1 Preparation of liposomes and RGD-conjugated liposomes

Liposome formulation was optimised by varying the amounts of different excipients and drugs, and changing the sonication conditions (S4; Table S1. The optimized liposomes containing DSPC and cholesterol in the molar ratio of 1:0.5 (LP-3) was selected and named LP hereafter for further RGD peptide conjugation, *in vitro* and *in vivo* studies. EDC-NHS and maleimide-thiol reaction mechanisms were applied for conjugation of RGD peptide by adopting post-insertion method. After the size exclusion chromatography, an appreciable extent (89.5±2.8% of initial amount) of lipid was recovered by Stewart's assay.

In the preformulation studies, FTIR and DSC studies confirmed that the excipients (DSPC and cholesterol) are compatible with ASPM in physical mixture as well as in the formulations. In DSC analysis, interestingly the melting point of cholesterol appeared at 149.52 ºC, which found to be decreased in placebo liposomes may be due to moistening effect of DSPC (Victoria and David, 2003). Details of FTIR and DSC analyses are given in Supplementary Information (Section S1 as well as Figure S1 and S2).

3.2 Characterization of conjugated and unconjugated liposomes

3.2.1 Conjugation confirmation by FTIR

In FTIR spectrum of DSPE-PEG-COOH, peaks at wavenumber 2854 and 2916 cm^{-1} corresponded to alkane C-H groups. Peaks at 3398 and 3552 cm^{-1} corresponded to –OH group and –NH group, respectively. The peak at wavenumber 1734 cm^{-1} is due to –C=O of ester, whereas –C=O of acid was observed at 1654 cm^{-1} (Figure *S3A*). In FTIR spectrum of DSPE-PEG-RGD (Figure *S3B*), -C=O of –COOH was not observed; instead, an amide –C=O peak at 1670.35 cm^{-1} was observed. Unconjugated liposomes (no drug) showed sharp ester –C=O peak at 1734.01 cm^{-1} (Figure *S3C*). Down to this wavenumber, two small peaks matching to acid –C=O (1654.92 cm^{-1}) and amide

–C=O (1546.91cm^{-1}) were observed. The peaks at wavenumbers 2926.01 cm^{-1} and 2856.58 cm^{-1} were due to alkane –CH groups. –NH and -OH groups of DSPE-PEG-COOH (linker) and –OH group of cholesterol showed a broad peak at ≈3200 cm^{-1}. In FTIR spectrum of LP-CONH-RGD liposomes (Figure *S3D*), alkane –CH groups were observed at 2926.01 cm^{-1} and 2854.65 cm^{-1}. Sharp ester –C=O peak, same as in unconjugated liposomes was observed at 1737.86 cm^{-1} and amide –C=O was observed at 1654.92 cm^{-1}. The broad peak of –NH and –OH groups were observed at 3387 cm^{-1} and 3248.13 cm^{-1} in LP-CONH-RGD. In the FTIR analysis, unconjugated liposomes (no drug) showed sharp ester –C=O peak may be due to the contribution of four ester –C=O groups (two from DSPC and two from linker) whose similar neighbouring groups resulted in null neighbouring effect and the peak sharpness. In FTIR spectrum of LP-CONH-RGD liposomes, because of four –CONH groups (two –CONH group of RGD, one –CONH group of a linker and one –CONH bond formed as a result of conjugation between linker and RGD) with different neighbouring groups, its shape was distorted. Also, the broad peak of –NH and –OH groups in LP-CONH-RGD liposomes confirmed the successful conjugation of RGD peptide.

3.2.2 Physico-chemical properties of conjugated and unconjugated liposomes

The various physicochemical properties of conjugated liposomes are shown in Table 1. The particle size of liposomes with linkers increased compared to liposomes without the linker. Moreover, conjugated liposomes LP-CONH-RGD and LP-MAL-RGD liposomes did not show a considerable increase in particle size compared to liposomes with linker. Observed zeta potential values of plain liposomes (LP-3), liposomes with only DSPE-PEG-COOH linker and RGD conjugated liposomes (LP-CONH-RGD) were in range of 43-52 mV.

The maleimide functionalized liposomes (LP-MAL) showed the particle size and PDI of 103.0±6.0 nm and 0.218±0.012, respectively while the zeta potential of LP-MAL and LP-MAL-RGD was in the range of 24-28 mV. The LP-DTPA liposomes and LP-MAL-RGD-DTPA liposomes showed a particle size of 104.3±2.5 nm and 109.0±1.9 nm and zeta potential values of -24.3±0.6 mV and -22.4±0.3 mV respectively. Entrapment efficiency was almost similar in all the liposomes and ranged from 47.4 to 52.2%.

The results of stability assessment of LP-3 and LP-CONH-RGD revealed that all the tested liposomes were found to be stable at 5±3 °C with an average particle size <150 nm and drug content of >90 % up to 6 months of storage. However, at 25±2°C/60±5% RH, the average particle size was maintained <300 nm up to 60 days and drug content was >90% up to 3 months.

Table 1. Physico-chemical properties of liposomes

Formulations		Drug	Label	Size[a] (nm)	PDI[a]	ZP[a] (mV)	EE[b] (%)	Peptide loading[c]
Plain liposomes	LP	✓	–	97.7± 1.5	0.216± 0.068	-51.2± 3.9	52.2± 3.6	-
	LP-DiI	-	DiI	107.2± 0.9	0.217± 0.017	7.2± 0.5	-	-
-COOH functionalized liposomes	LP-COOH	✓	–	108.5± 2.6	0.236± 0.031	-43.7± 4.6	51.3± 4.8	-
	LP-CONH-RGD	✓	–	109.7± 3.5	0.235± 0.069	-45.2± 3.6	49.2± 5.1	RGD: 7.86 (61.3 mol%)
Maleimide functionalized liposomes	LP-MAL	–	–	103.0± 6.0	0.218± 0.012	-27.6± 3.6	-	-
	LP-MAL-RGD	–	–	101.1± 0.8	0.262± 0.019	-24.6± 1.3	-	RGDC: 7.24 (56.5 mol%)
	LP-DTPA	–	(RL[c]) DTPA	104.3± 2.5	0.213± 0.013	-24.3± 0.6	-	-
	LP-MAL-RGD-DTPA	–	(RL) DTPA	109.0± 1.9	0.199± 0.002	-22.4± 0.3	-	-
	LP-MAL-RGD-DiI	–	DiI	109.9± 1.7	0.270± 0.020	-2.1± 0.1	-	-

[a] Particle size and zeta potential were measured in deionized water by dynamic light scattering (DLS)
[b] EE (%) was measured by HPLC
[c] RL: Radiolabelled

3.2.3 XRD analysis

ASPM showed two characteristic peaks in the XRD pattern; an intense peak at a 2-theta value of 21.7º (intensity: ≈9000 cps) and another peak at 9.4º (Figure *S4A*). DSPC and cholesterol physical mixture showed a broad peak between 5° and 35° and the appearance of the halo region at the baseline (Figure *S4B*). Similarly, the mixture of DSPC, cholesterol and ASPM showed a broad peak in the region between 5° and 35° (Figure *S4C*) with a small sharp peak arising at top of the broad peak at a 2-theta value of about 21°. Placebo liposomes (LP-3 liposomes with no drug) (Figure *S4D*) and ASPM liposomes (LP-3 liposomes) (Figure *S4E*) showed almost similar XRD patterns without any intense peaks of ASPM. Plain ASPM showed a sharp peak with high intensity, indicating crystalline nature of drug. A physical mixture of DSPC and cholesterol is amorphous in nature as there is a broad peak without any intense peak. The XRD pattern of a physical mixture of DSPC, cholesterol, and ASPM showed a broad peak with a small intense peak indicating partial amorphization of the drug. The intense peak corresponds to ASPM found to be disappeared in the

XRD pattern ASPM liposomes (LP-3 liposomes) clearly suggest the possible amorphization of entrapped ASPM.

3.2.4 Transmission electron microscopy (TEM)

TEM images (Figure *S5A* and *S5B*) of unconjugated liposomes (LP-3) and RGD conjugated liposomes (LP-CONH-RGD) revealed spherical shaped vesicles of about 100 nm size.

3.3. In vitro drug release study

In *in vitro* drug release study by dialysis sac method, LP-3 liposomes showed 14.7±4.7% of ASPM release in pH 1.2 HCl solution within the first 2 h (Figure1A) . In pH 4.5 ammonium acetate buffer, 9.3±3.2% drug was released form LP-3 liposomes in 1 h. In pH 6.8 phosphate buffer, 54.7±2.8% drug was released in 6 h (Figure 1A); whereas in pH 7.4 phosphate buffer, 81.1±2.2% drug was released in 48 h (Figure 1B).

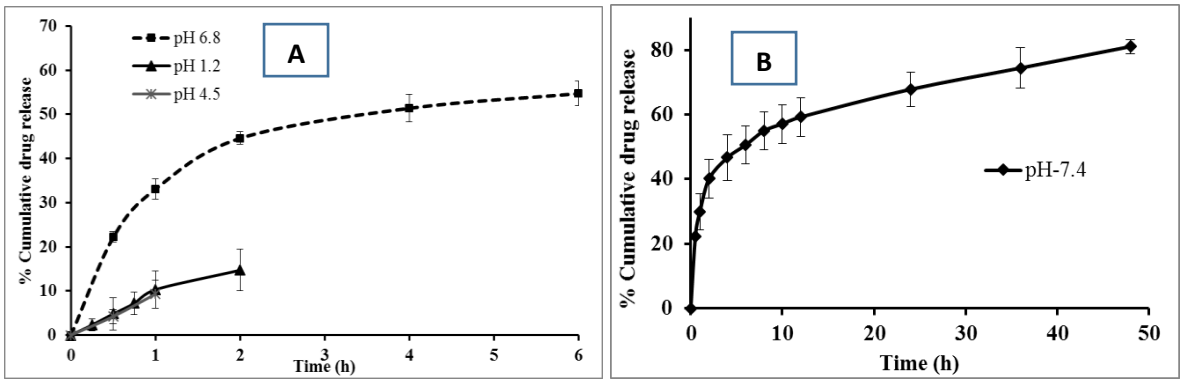

Figure 1. *In vitro* drug release study of ASPM from LP-3 liposomes in (A) pH 1.2 HCl, pH 4.5 acetate buffer and pH 6.8 phosphate buffer and (B) pH 7.4 phosphate buffer

3.4 In vitro uptake and permeability studies

Both mono and co-culture cells showed significantly (p<0.05) higher uptake of all the tested liposomes compared to free dye (Figure 2). The order of cell uptake found to be FITC tagged LP-CONH-RGD > FITC tagged LP-3 liposomes > free FITC. Liposomes attached with RGD peptide showed higher uptake into co-culture compared to mono culture. The viability of both mono and co-culture cells treated with these liposomal formulations was almost similar compared to free drug. More than 80% of cells were viable in both mono and co-culture even at a higher concentration of ASPM (1, 3, 10 and 15 µM/mL). LP-CONH-RGD liposomes showed a considerable increase in cell permeability (P*app* = 29.0±2.8 x10^{-6}) compared to unconjugated liposomes (LP-3 liposomes, P*app* = 26.2±1.8 x10^{-6}) and plain drug (P*app* = 4.1±0.3x10^{-6}) in monoculture. Similarly, in Caco2 and RajiB co-culture also, LP-CONH-RGD liposomes (P*app* = 44.2±2.4 x10^{-6}) showed further higher permeability than the LP-3 (P*app* = 34.5±1.7 x10^{-6}) and plain drug (P*app* = 5.0±0.2x10^{-6}). Cell viability and permeability results are shown in Table *S3*.

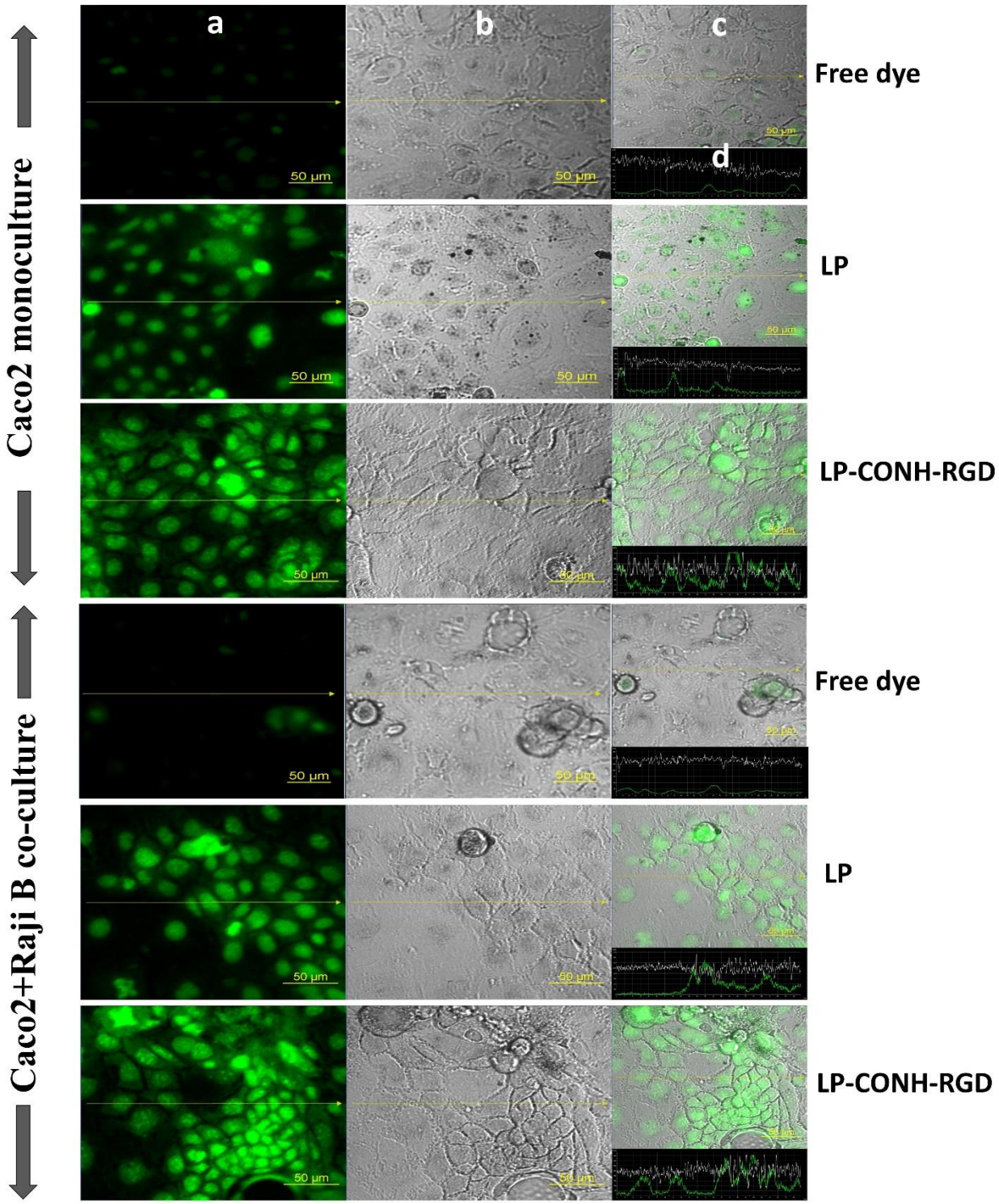

Figure 2. Uptake of free dye, LP-3 liposomes and LP-CONH-RGD liposomes by monoculture and co-culture. (a) Images under the green fluorescence channel; (b) Corresponding differential interface contrast images of cells; (c) Superimposition of (a) and (b); (d) Horizontal line series analysis of fluorescence along the yellow line

3.5. Ex vivo and in vivo studies

3.5.1. Ex vivo study: Everted ileum sac technique

LP-3 liposomes showed significant (p<0.05) increase in *P*app value (1 h: 55.5±2.46 x 10^{-5} cm/sec; 2 h: 37.0±4.3 x 10^{-5} cm/sec; 3 h: 31.6±1.2 x 10^{-5} cm/sec) compared to free drug (1 h: 32.2±3.0 x 10^{-5} cm/sec; 2 h: 25.3±4.4 x 10^{-5} cm/sec; 3 h: 21.4±4.0 x 10^{-5} cm/sec). LP-CONH-RGD liposomes showed enhanced permeation (1 h: 67.9±3.6 x 10^{-5} cm/sec; 2 h: 47.1±3.5 x 10^{-5} cm/sec; 3 h: 38.5±3.2 x 10^{-5} cm/sec) through everted ileum sac compared to LP-3 liposomes (Figure 3A).

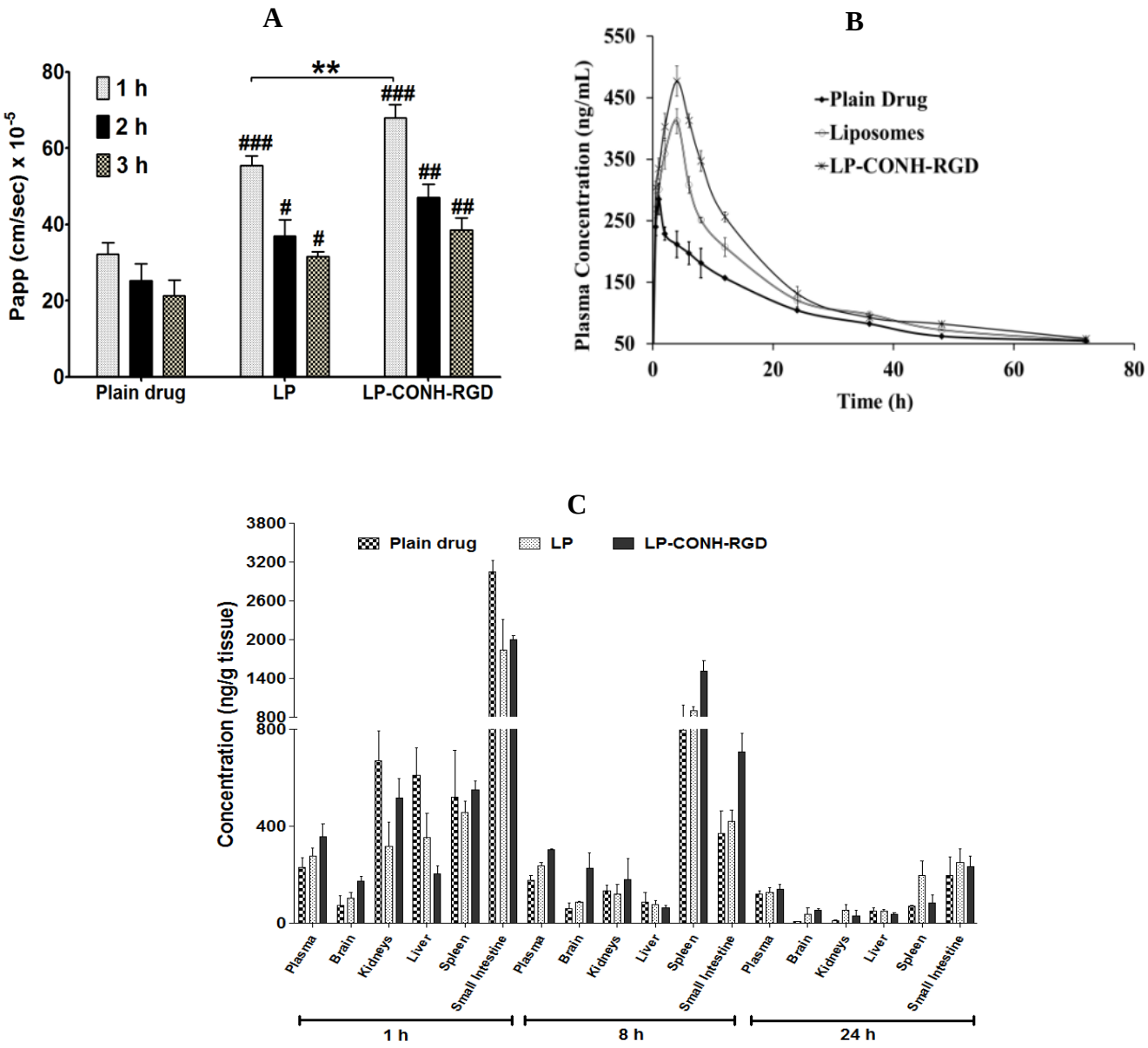

Figure 3. Results of ex vivo permeability, pharmacokinetics and tissue distribution
(A) Permeability of plain drug, LP-3 liposomes and LP-CONH-RGD liposomes through rat ileum. (B) Plasma concentration *vs.* time profile. (C) Tissue distribution profile.

3.5.2. Pharmacokinetics study

The mean plasma concentration-time profile of plain ASPM, LP-3 liposomes and LP-CONH-RGD liposomes in rats after oral administration at ASPM equivalent dose of 15.8 mg/kg is shown in Figure 3B and the respective pharmacokinetic parameters are given in Table 2. The AUC_{0-t} of the liposomal formulations was much greater than that of the ASPM solution indicating greater bioavailability of ASPM in liposomal form. The C_{max} value was improved by ≈1.5 times with all the liposomal formulations compared to plain drug and conjugated liposomes showed comparatively higher C_{max} values than the un-conjugated liposomes (LP-3). The half-life values of drug was increased for LP-3 liposomes (≈1.3 times) and LP-CONH-RGD liposomes (≈1.7 times) in comparison with plain drug.

Table 2. The pharmacokinetic parameters of plain drug, LP-3 liposomes and LP-CONH-RGD liposomes when administered orally in rats.

Parameters	Plain drug	LP-3 Liposomes	LP-CONH-RGD Liposomes
Cmax (ng/mL)	284.93 ± 14.20	412.11 ± 19.86	477.03 ± 34.26
Tmax (h)	1.00 ± 0.00	4.00 ± 0.00	4.00 ± 0.00
AUC_{0-t} (h*ng/mL)	7309.06 ± 458.23	9347.09 ± 440.97 *	10745.05 ± 622.48 *$
$AUC_{0-\infty}$ (h*ng/mL)	9792.10 ± 356.82	12741.22 ± 377.23 *	15214.98 ± 659.52 *$
$t_{1/2}$ (h)	31.60 ± 2.10	42.50 ± 2.30	53.10 ± 0.90
Vd (mL)	18423.08 ± 1875.70	19028.45 ± 1608.00	19927.85 ± 1191.15 *
CL (mL/h)	403.74 ± 14.70	310.20 ± 9.18	259.86 ± 11.26
Ke (1/h)	0.0220 ± 0.0015	0.0163 ± 0.0009	0.0131 ± 0.0002
MRT (h)	26.20 ± 0.70	23.80 ± 0.20	22.60 ± 0.30

* $p < 0.05$= statistically different from respective parameter of ASPM
$ $p < 0.05$= statistically different from respective parameter of LP-3 liposomes
# $p < 0.05$= statistically different from respective parameter of LP-CONH-RGD

3.5.3. Tissue distribution study

Tissue distribution of the plain drug, LP-3 liposomes and LP-CONH-RGD liposomes after 1 h, 8 h and 24 h of oral administration are shown in Figure 3C. Compared to the plain drug, all the liposomes showed a high concentration of drug in the brain at all three-time points. Among liposomes, LP-CONH-RGD liposomes showed higher drug concentration in the brain than LP-3. LP-CONH-RGD liposomes showed considerably less distribution of the drug in the liver at all the time points compared to plain ASPM and LP-3 liposomes. LP-CONH-RGD liposomes showed a higher concentration of drug in the spleen at 1 h and 8 h but less concentration at 24 h compared to LP-3 liposomes.

3.5.4. Pharmacodynamic study

Intraperitoneal administration of L-dopa and carbidopa induced hyper LMA in the rats (Figure 3D). Administration of plain drug brought down the LMA less than the normal values at all the time points up to 3 h. This effect was more prominent with all the liposomes administered animals. All the tested liposomes showed a remarkable reduction in L-Dopa and carbidopa induced LMA compared to the plain drug (Figure 3D). However, the antipsychotic effect was maximum in the rats administered with LP-CONH-RGD liposomes.

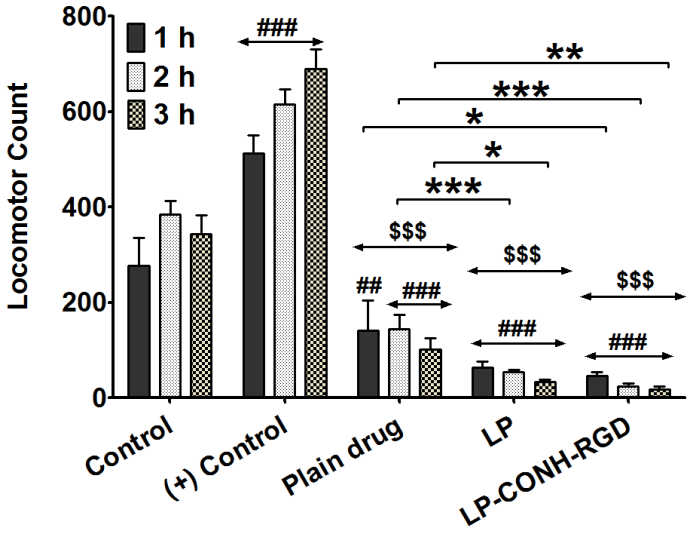

Figure 4. Results of pharmacodynamics studies of liposomes
Locomotor activity in control (normal untreated group), (+) Control (Positive control *i.e.* L-Dopa and carbidopa treated group), plain drug, LP-3 liposomes and LP-CONH-RGD liposomes. ### $p<$ 0.001, ## $p<$ 0.01, # $p<$ 0.05= statistically different compared to respective time of plain drug in everted sac ileum method or control in pharmacodynamic study. $$$ $p<$ 0.001= statistically different compared to respective time of positive control in pharmacodynamic study. *** $p<$ 0.001, ** $p<$ 0.01, * $p<$ 0.05= statistically different form each other.

3.9.5. Assessment of targetability of RGD conjugated liposomes to Peyer's patches

3.9.5.1. Whole-body 3D SPECT/CT imaging and gamma scintigraphy

The radiolabeling efficiency was examined using TLC. TLC strips showed the movement of free [^{111}In]EDTA along the solvent front; whereas the [^{111}In] bound to liposomes remained at the application point (Figure *S6A*). Fractions of [^{111}In]LP and [^{111}In]LP-MAL-RGD were collected after passing through PD-10 columns and the fractions did not show free [^{111}In] were pooled for *in vivo* studies. After 24 h of incubation in PBS or 50 % serum, [^{111}In]liposomes were found to be completely stable in both PBS and in serum for 24 h as no free [^{111}In] moved along with the solvent front was observed (Figure *S6B*).

Dynamic biodistribution of [^{111}In]LP and [^{111}In]LP-MAL-RGD was assessed by whole-body SPECT/CT imaging after oral administration. As shown in Figure 5A, both liposomes reached stomach during the first 40 min following gavaging and the signals from [^{111}In]LP-MAL-RGD could also be detected in small intestine. At 4 h post administration, both liposomes entered small intestine and cecum. At 24 h, most of the [^{111}In]LP-MAL-RGD was excreted with low signals detected remain in the GI tract while some [^{111}In]LP still remained in the intestine.

After 1 h and 3 h of oral administration of [^{111}In] LP-MAL-RGD, the rats were sacrificed and the organs were isolated. The extent of radioactivity in different isolated organs is shown in Figure 5B. In general, most of the [^{111}In]LP-MAL-RGD were excreted from the body at 1 h and 3 h post oral administration (< 1 % ID). The highest radioactivity was observed in the small intestine even though they were emptied and thoroughly flushed with buffer before gamma counting.

The specific uptake of [^{111}In]LP-MAL-RGD in small intestine was further assessed by examining the radioactivity in the Peyer's and non-Peyer's patches segments. It was found that at 1 h, the total radioactivity was considerably higher in Peyer's patches compared to non-Peyer's patches regions, indicating the targetability of [^{111}In] LP-MAL-RGD to Peyer's patches (Figure 5C). The uptake in both regions were comparable at 3 h post administration.

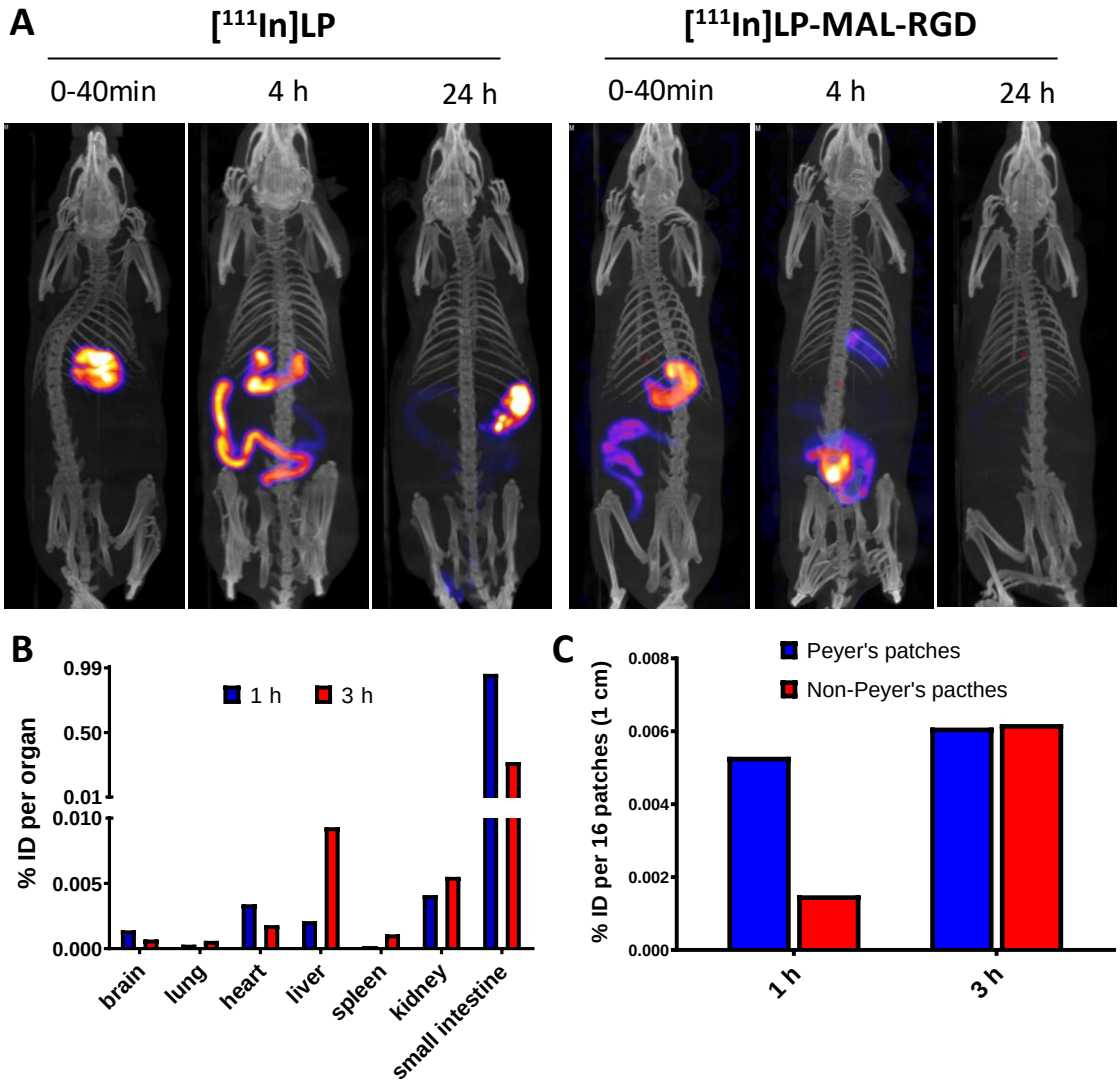

Figure 5. ***In vivo*** **whole body SPECT/CT imaging and biodistribution studies of [^{111}In]LP and [^{111}In]LP-MAL-RGD in rats following oral administration. (A)** SPECT/CT images of [^{111}In]LP and [^{111}In]LP-MAL-RGD after and at 4 h and 24 h post oral administration. **(B)** Accumulation of [^{111}In]LP-MAL-RGD in selected organs at 1 h or 3 h post oral administration. (n=1) **(C)** Uptake of [^{111}In]LP-MAL-RGD in Peyer's and non-Peyer's patches from small intestine (16 patches each) at 1 h or 3 h post oral administration. Wistar rats were orally given [^{111}In]LP or [^{111}In]LP-MAL-RGD. For biodistribution studies, the radioactivity from each organ and tissue sampled at 1 h or 3 h post administration was measured by gamma scintigraphy. Data are expressed as percentage injected dose (%ID) per organ or per type of patches respectively.

3.9.5.2. Ex vivo optical imaging

Overnight fasted rats were administered orally with LP-DiI or LP-MAL-RGD-DiI and the rats were sacrificed and small intestine was dissected out at 3 h post administration. The intestine was cut into 1 cm segments in length and categorized into two groups with or without Peyer's patches and imaged by IVIS optical imaging system as shown in Figure 6A, the fluorescence signals of LP-DiI were detected in some of segments of both non-Peyer's patches and Peyer's patches at 1 h post

administration, but negligible fluorescence was observed on either segment at 3 h. In the case of LP-MAL-RGD-DiI, significant higher and more localised signals were detected in the segments containing Peyer's patches compared to non-Peyer's patches segments at 1 h. At 3 h, some signals although to a lesser extent, could still be detected in the Peyer's patches-containing segments. Quantitative analysis on the images further confirmed that LP-MAL-RGD-DiI exhibited higher accumulation in small intestine than non-targeted LP-DiI and the uptake in the Peyer's patches-containing segments were significantly higher than the non-Peyer's patches segments (Figure 6B).

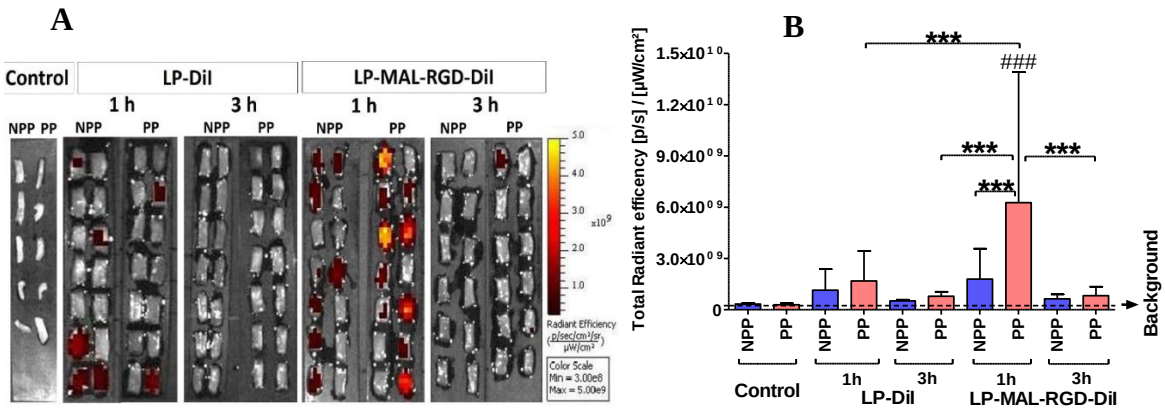

Figure 6. ***In vivo*** **fluorescent imaging and quantification of small intestinal segments** (A) Fluorescence images of rat intestinal segments at different time intervals treated with LP-DiI liposomes and LP-MAL-RGD-DiI liposomes. (B) Total radiant efficiency of rat intestinal segments at different time intervals treated with LP-DiI liposomes and LP-MAL-RGD-DiI liposomes. ### $p<$ 0.001= statistically different compared to control; *** $p<$ 0.001= statistically different from each other.

Another *ex vivo* study was performed by direct exposure of LP-MAL-RGD-DiI to small intestine to examine the Peyer's patches targetability of RGD conjugated liposomes. Excised rat intestine was infused with LP-MAL-RGD-DiI for 1 h or 3 h, following by optical imaging the entire intestine and its segments with/without Peyer's patches. Figure 7A clearly shows that a greater extent of fluorescence was observed for the intestine and its segments after the incubation of LP-MAL-RGD-DiI for 3 h compared to 1 h. Nevertheless, in either conditions, higher fluorescence signals were measured in Peyer's patches segments than the segments without Peyer's patches. This observation clearly suggests the Peyer's patches targeting of RGD conjugated liposomes which is also confirmed by quantitative analysis shown in Figure 7B.

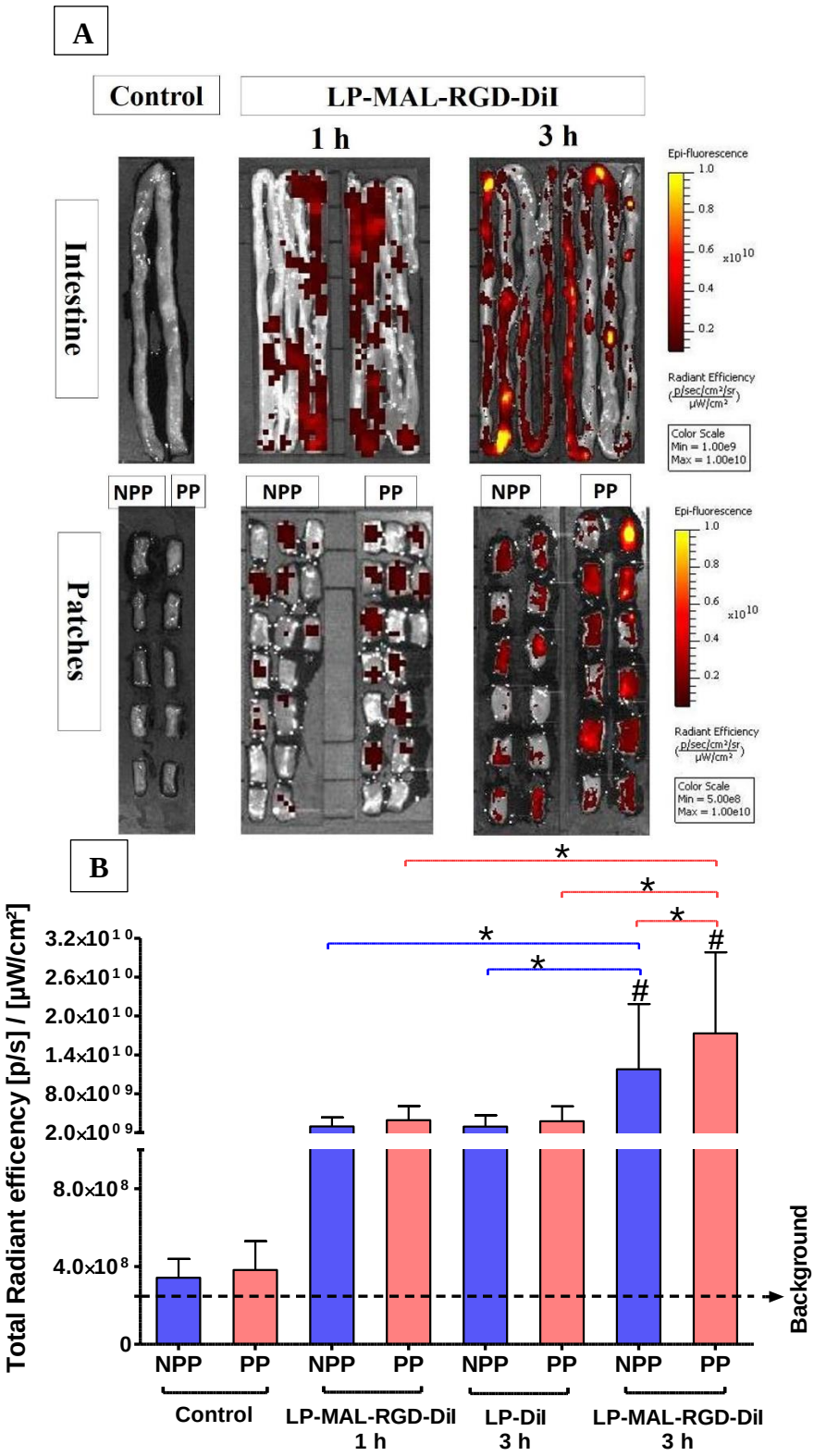

Figure 7. Results of ex vivo fluorescent imaging of small intestine and its segments (A) Representative ex vivo fluorescence images of small intestine and patches (PP= Peyer's patches and NPP= non-Peyer's patches). (B) Fluorescence quantitative result of patches. # $p < 0.001$= statistically different compared to respective patches of control. * $p < 0.05$.

4. Discussion

The present work prepared Peyer's patches targeting liposomal ASPM *via* RGD peptide conjugation. In several previous reports, RGD peptide has been used ligand for targeting the Peyer's patches (Lundquist & Artursson, 2016; Gullberg et al., 2006). The formulated liposomes were extensively characterized by several techniques such as DSC, FTIR spectroscopy, and XRD. The results suggested that there was no interaction between ASPM and the excipients used and amorphization of ASPM was also depicted. Optimized liposomes containing DSPC and cholesterol in the molar ratio of 1:0.5 (LP-3) was selected for conjugating RGD peptide. DSPE-PEG2000-COOH is a carboxylic acid functionalized PEG-lipid which acts as a linker for attachment of amine-containing ligand to the liposomes. DSPE-PEG2000-COOH was added during the thin film formation step in the preparation of liposomes at the molar ratio of 2:0.02 of DSPC and linker. EDC-NHS and maleimide-thiol reaction mechanism were applied for conjugation and RGD ligand was attached by adopting the post-insertion method. In the post-insertion method, only the outer surface of liposomes is being modified without any changes to interior space of vesicle thereby allowing maximum entrapment of drug.

The higher particle size of liposomes with linker was probably because of the long PEG chain (MW: 2000) of the linker. There was no considerable increase in particle size of LP-CONH-RGD liposomes and LP-MAL-RGD liposomes compared to unconjugated liposomes. The size of the liposomes observed with TEM was less than that observed with DLS; however the difference in size was not substantial, which may be attributed to the fact that the effect of solvation/ hydration sphere is negligible in case of lipidic nanoparticles (Zheng et al 2016; Ribeiro et.al, 2018).

The plain liposomes (containing DSPC, cholesterol and ASPM) showed higher zeta potential value which may be because of negatively charged lipids. In the liposomes with only DSPE-PEG-COOH linker, low zeta potential value was observed which may be due to steric effect of PEG chain. Thus negative charge contributed by DSPE-PEG-COOH is balanced by charge shielding effect of PEG chain, although the net zeta potential is in the negative side (Nakamura et al., 2012). The slight increase in zeta potential value of LP-CONH-RGD compared to liposomes with linker alone may be due to the carboxylic groups of RGD. All the liposomes showed similar trend for the entrapment efficiency. The higher size of the maleimide functionalized liposomes may be due to vesicle aggregation (Loughrey et al., 1990).

Stability studies clearly indicate that the developed liposomes (Plain and conjugated) were found to be stable with respect to size, PDI and drug content for 6 months at 5±3°C and for 60 days at 25±2°C/60±5% RH. Considering the necessity of particle size ≤ 200 nm for targeting to the intestinal lymphatic system, liposomes can be considered stable up to 30 days at 25±2°C/60±5% RH

and up to 6 months at 5±3°C. The NTA analysis of LP-3 and LP-MAL-RGD suggested that there no significant decrease in the particle concentration per mL of the volume of the buffer.

While conducting the *in vitro* drug release study, attention was given to the duration of drug release in a specific medium mimicking the gastro-intestinal emptying time. The results clearly indicate that the drug release from the liposomes takes place in a sustained manner over the duration of 48 h.

It is reported that Caco2 cells can differentiate to have M cell-like morphological structures with similar phenotype after *in vitro* co-culture with murine Peyer's patches derived lymphocytes or human B lymphoma cell lines (Miller et al., 2007). Monoculture of Caco2 cell line was used to depict the transport of liposomes across the intestinal epithelium. *In vitro* cell uptake study gives an idea about the *in vivo* interaction of liposomes with the intestinal epithelial cells. The significantly higher uptake of the tested liposomes by mono and co-culture cells as compared to the free dye could be due to nanosize and endocytosis uptake pathway. As reported earlier, the nanoformulations which exhibit the size < 200 nm shown higher cellular uptake as it can efficiently cross the mucus barrier and taken up by the epithelial cells through endocytosis mechanism (Fang et al., 2015). Liposomes attached with RGD peptide showed higher uptake into co-culture compared to mono culture. This may be because of the interaction of RGD peptide with M cells, which eventually take up the liposomes by receptor-mediated endocytosis. This clearly suggests the precise targetability of the liposomes conjugated with RGD peptide to β1 integrins expressed on the M cells.

The higher permeability of the treated liposomes across the mono and co-cultures may be due to their lipidic nature. ASPM exhibits solubility (dissolution) limited absorption and less permeation across the intestinal epithelium. Due to the nano-size and physiological resemblance, the liposomes are generally taken up by the cells at a greater extent compared to the pure drug (Khan et al., 2015). The high permeability of LP-CONH-RGD liposomes may be due to the presence of RGD peptide on the surface of the liposomes, which specifically target the β1 integrins receptors expressed on the cells. It also has been reported that RGD-peptide disrupts the interaction of the cytoskeleton with the plasma membrane through an unknown integrin-like protein and thus causes the disruption of cytoplasmic architecture and inhibition of deplasmolysis resulting in loss of membrane integrity (Hohenberger et al., 2011).

In the Everted ileum sac technique, LP-3 liposomes showed significant (p<0.05) increase in *P*app value compared to free drug. This could be due to the lipidic nature of liposomes and the interaction of phospholipid head groups with mucus glycoproteins that results in restructuring of mucous membrane thereby showing greater permeability (Lavanya et al., 2016). LP-CONH-RGD showed enhanced permeation compared to LP-3 liposomes which could be because of RGD-M cell β1 integrin interaction that may cause receptor-mediated endocytosis.

In pharmacokinetics study, AUC_0-t of all the liposomal formulations found to be much greater than that of the ASPM solution indicating greater bioavailability of ASPM in liposomal form. LP-3 liposomes showed ≈1.3 times higher increase in half-life compared to plain drug. On the other hand, LP-CONH-RGD liposomes showed a further increase in the half-life of the drug (1.7 times higher than the pure drug). These observations indicate the prolonging of the stay of ASPM in the body when administered in the form of liposomes. This was further supported by lower elimination rate constant values observed with liposomes than that observed with plain drug. Among the different liposomes, LP-CONH-RGD showed better pharmacokinetic profile compared to LP-3. This could be due to the interaction of the attached ligands (RGD peptide) to the liposomes which aid in better interaction between liposomes and intestinal membrane by targeting β1 integrins of M cells of Peyer's patches and thereby increasing their uptake directly into the intestinal lymphatic system. In a previous study, glycol chitosan coated NLCs loaded with ASPM showed better pharmacokinetic and safety profile via intranasal route (Singh et al., 2018). Nano-transfersomes loaded with ASPM also showed better pharmacokinetics profile than that of pure drug via transdermal administration (Shreya et al., 2016). In other studies, NLCs and Self-micro-emulsifying drug delivery systems showed improved absorption and pharmacokinetics profile of ASPM (Patel et al., 2019a; Patel et al., 2019b).

In tissue distribution study, all the liposomes showed high concentration of drug in the brain at all three-time points (1, 8 and 24 h) indicate that the more drug was available from the liposomes in the systemic circulation for ready access to the brain. The ASPM concentration in the brain was in the order of LP-CONH-RGD > LP-3 liposomes > plain drug. LP-CONH-RGD liposomes showed the lowest distribution of drug in liver which may be due to the possible interaction between the conjugated ligands on the liposomal surface and the intestinal membrane, resulting in higher absorption of the drug directly into the systemic circulation via lymphatic system bypassing the first pass effect. A higher concentration of drug in the brain may be attributed to bypassing the first pass effect.

Due to the effective pharmacokinetics and tissue distribution profiles of the LP-CONH-RGD liposomes, the L-Dopa and carbidopa induced LMA in rats found to be reduced as compared to the plain drug. The excellent reduction LMA of rats was observed in case of LP-CONH-RGD as compared to the LP-3, which may serves as excellent antipsychotic treatment.

The dose of ASPM (15.8 mg/kg) in rats was selected considering the variable bioavailability of ASPM via oral as well as buccal routes (≈2% and 35% respectively). Ten mg of total daily dose when administered via buccal route resulted in a bioavailability of 35%. Hence in order to achieve same oral bioavailability as that observed with buccal dose, the oral dose needs to be ≈ 17.5 times higher than the buccal dose. The rat dose, when extrapolated from human dose, was calculated to be

≈ 15.8 mg/kg (Nair and Jacob, 2016). In a previous report, pharmacological response was observed even at comparatively less dose of ASPM in rats (Patel et al., 2019a). In another report, a wide range of oral bioavailability (20 to 65%) has been reported for ASPM in rats (https://www.accessdata.fda.gov/drugsatfda_docs/nda/2009/022117s000_PharmR.pdf). All these details suggest that ASPM may exhibit a pharmacological response at a broad dose range, which may be due to its highly variable bioavailability, leading to inconsistent therapeutic effect (Citrome, 2014).

With respect to pharmacokinetics, pharmacokinetics and tissue distribution studies, conjugated liposomes of this study showed better performance when compared with ASPM NLCs of our previous study (Managuli et al, 2019). This could be attributed to combined uptake mechanisms *viz.*, improved uptake by precise targetability of conjugated liposomes to intestinal Peyer's patches in conjunction with chylomicron assisted pathway. It is evident from the cell uptake assessment in the present study in which the conjugated liposomes showed considerable uptake in Caco2 as well as in co-culture of RajiB and Caco2 cells, though uptake was little bit higher in co-culture.

For *in vivo* gamma scintigraphy, DSPE-DTPA was incorporated into the liposome formulation and used as a linker for [^{111}In] labeling. TLC analysis confirmed the high radiolabelling efficiency and good labelling stability. At 1 h and 3 h post oral administration, the %ID in all the organs was low which may be due to possible degradation of some liposomes by stomach acidic condition, bile salts, and lipase (Hua, 2014). In comparison with organs tested, , the maximum radioactivity of [^{111}In]LP-MAL-RGD was observed in the small intestine as it is the organ of retention of ingested matter. Liver and spleen showed higher radioactivity at 3 h compared to 1 h which may be because of faster intestinal lymphatic uptake and later once in blood, lipid accumulates in liver and spleen. The radioactivity in kidneys suggests the high renal elimination of radioactive compound. Interestingly, the brain also showed extensive radioactivity within 1 h indicating the faster absorption of radiolabelled liposomes through the intestinal lymphatic system bypassing the first pass effect. The avoidance of first pass effect is supported by less radioactivity in the liver at 1 h compared to 3 h.

The targetability of [^{111}In]LP-MAL-RGD to Peyer's patches was also assessed. At 1 h, the radioactivity was considerably higher in Peyer's patches indicating the greater uptake of [^{111}In]LP-MAL-RGD by Peyer's patches. This observation, along with greater radioactivity in brain and less radioactivity in liver at 1 h, clearly supports the targetability of RGD conjugated liposomes to intestinal lymphatic system and there by bypassing the first pass effect in the liver. The imaging results clearly showed that less fluorescence was observed in the case of LP-DiI liposomes on rat's intestinal Peyer's patches as well as non-Peyer's patches segment; whereas, LP-MAL-RGD-DiI liposomes showed higher fluorescence at the Peyer's patch segments than the non-Peyer's patch

segments. This may be due to precise targeting ability of RGD peptide conjugated liposomes to the Peyer's patches. These observations were further supported by *ex vivo* optical imaging study. By exposing rat intestine with LP-DiI and LP-MAL-RGD-DiI liposomes externally, similar results were obtained where maximum fluorescence intensities were observed in rat's intestinal Peyer's patch segments than non-Peyer's patches. In the experiments with intestinal tissues, it was found that the permeability of the nanoparticles decorated with RGD-peptide was 5 times higher in tissue specimens containing Peyer's patches compared to normal villous epithelium (Gullberg et al., 2006). It has also been demonstrated that RGD peptide binds to exposed integrins and RGD peptide takes advantage of this attribute to target M cells (Garinot et al., 2007).

5. Conclusions

In this study, RGD peptide conjugated ASPM loaded liposomes were prepared in order to target the β1 integrins on intestinal M cells in order to improve the lymphatic delivery of ASPM. The liposomes exhibited excellent physicochemical properties. The *in vitro* drug release study suggested the sustained release of drug from the liposomes. Liposomes showed excellent uptake by Caco2 and RajiB co-culture cells. More than 80% cells were viable in MTT assay of liposomes. The apparent permeability of RGD conjugated liposomes in cells and in rat ilium was found to be highest. Liposomes improved the pharmacokinetics and efficacy profile of ASPM. Gamma scintigraphy studies proved the targetability of ^{111}In labeled RGD conjugated liposomes (LP-MAL-RGD) to the Peyer's patches of intestine of rats. Similarly, *in vivo* and *ex vivo* imaging showed the successful targetability of liposomes to the Peyer's patches.

6. Acknowledgements

The authors gratefully acknowledge Science and Engineering Research Board (SERB), Department of Science and Technology, Govt. of India, New Delhi for funding the research project. Authors are thankful to British Council and DBT, Government of India for providing Newton-Bhabha Fellowship to Dr Renuka S. Managuli. KAJ acknowledges funding from Worldwide Cancer Research (12−1054). Authors are grateful to Manipal Academy of Higher Education, Manipal, India for providing necessary facilities and to MSN Organic Ltd., Hyderabad, India and Orbicular Pharmaceutical Technologies Ltd., Hyderabad, India for providing gift samples of few of the materials used in the study. The authors would like to acknowledge the support from Dr Jane Sosabowski at Barts Cancer Institute, Queen Mary University of London (UK), for her assistant on SPECT/CT imaging. Authors also thank Dr Yueting Li, a visiting post-doctoral research fellow at King's College London from Guizhou Medical University (China), for her assistant in animal work. Farid Faruqu was funded by the Malaysian government agency Majlis Amanah Rakyat (MARA).

7. References:

Citrome, L., 2014. Asenapine review, part I: chemistry, receptor affinity profile, pharmacokinetics and metabolism, Expert Opinion on Drug Metabolism & Toxicology, 10, 893-903.

Clark, M.A., Hirst, B.H., Jepson, M.A., 1998. M-Cell Surface β1 Integrin Expression and Invasin-Mediated Targeting of Yersinia pseudotuberculosis to Mouse Peyer's Patch M Cells. Infect. Immun. 66, 1237-1243.

Derakhshandeh, K., Hochhausa, G., Dadashzadehc, S., 2011. In-vitro Cellular Uptake and Transport Study of 9-Nitrocamptothecin PLGA Nanoparticles across Caco-2 Cell Monolayer Model. Iran. J. Pharm. Res. 10, 425-434.

Fang, G., Tang, B., Chao, Y., Zhang, Y., Xu, H., Tang, X., 2015. Improved oral bioavailability of docetaxel by nanostructured lipid carriers: in vitro characteristics, in vivo evaluation and intestinal transport studies. RSC Adv. 5, 96437-96447.

Fievez V, Plapied L, des Rieux A, Pourcelle V, Freichels H, Wascotte V, Vanderhaeghen ML, Jerôme C, Vanderplasschen A, Marchand-Brynaert J, Schneider YJ, Préat V. Targeting nanoparticles to M cells with non-peptidic ligands for oral vaccination. Eur J Pharm Biopharm. 2009, 73(1):16-24.

Gamboa, J.M., Leong, K.W., 2013. In vitro and in vivo models for the study of oral delivery of nanoparticles. Adv. Drug Deliv. Rev. 65, 800-810.

Garinot M, Fiévez V, Pourcelle V, Stoffelbach F: des Rieux A, Plapied L, Theate I, Freichels H, Jérôme C, Marchand-Brynaert J, Schneider Y-J, Préat V: PEGylated PLGA-based nanoparticles targeting M cells for oral vaccination. J Control Release 2007, 120:195-204

Gullberg E, Keita AV, Salim SY, Andersson M, Caldwell KD, Söderholm JD, Artursson P. Identification of cell adhesion molecules in the human follicle-associated epithelium that improve nanoparticle uptake into the Peyer's patches. J Pharmacol Exp Ther. 2006, 319 (2): 632-639

Hohenberger, P., Eing, C., Straessner, R., Durst, S., Frey, W., Nick, P., 2011. Plant actin controls membrane permeability. Biochim. Biophys. Acta 1808, 2304-2312.

Hua, S., 2014. Orally administered liposomal formulations for colon targeted drug delivery. Front. Pharmacol. 5, 1-2.

Jung, C., Hugot, J.P., Barreau, F., 2010. Peyer's Patches: The Immune Sensors of the Intestine. Int. J. Inflam. 2010, 1-12.

Kapadia, Y.D., Sodha, H.P., Patel, V.P., 2013. Formulation development and evaluation of sublingual film of asenapine maleate. Pharma Science Monitor 4, 190-209.

Khan, S., Baboota, S., Ali, J., Khan, S., Narang, R.S., Narang, J.K., 2015. Nanostructured lipid carriers: An emerging platform for improving oral bioavailability of lipophilic drugs. Int. J. Pharm. Investig. 5, 182-191.

Kulkarni, J.A., Avachat, A.M., 2017. Pharmacodynamic and pharmacokinetic investigation of cyclodextrin-mediated asenapine maleate in situ nasal gel for improved bioavailability. Drug Dev Ind Pharm 43(2), 234–245.

Lavanya, N., Muzib, Y.I., Aukunuru, J., Balekari, U., 2016. Preparation and evaluation of a novel oral delivery system for low molecular weight heparin. Int. J. Pharma. Investig. 6, 148-157.

Loughrey, H.C., Wong, K.F., Choi, L.S., Cullis, P.R., Bally, M.B., 1990. Proteinliposome conjugates with defined size distributions. Biochimica et Biophysica Acta, 1028, 73-81.

Lundquist P, Artursson P. Oral absorption of peptides and nanoparticles across the human intestine: Opportunities, limitations and studies in human tissues, Advanced Drug Delivery Reviews, 2016, 106: 256-276

Mabbott, N.A., Donaldson, D.S., Ohno, H., Williams, I.R., Mahajan, A., 2013. Microfold (M) cells: important immunosurveillance posts in the intestinal epithelium. Mucosal Immunol. 6, 666-677.

Managuli, R.S., Raut, S.Y., Reddy, M.S., Mutalik, S. 2018. Targeting the intestinal lymphatic system: A versatile path for enhanced oral bioavailability of drugs. Expert. Opin. Drug. Deliv. 15(8), 787-804.

Managuli, R.S., Wang, J.T., Faruqu, F.N., Kushwah, V., Raut, S.Y., Shreya, A.B., Al-Jamal, K.T., Jain, S., Mutalik, S. 2019. Asenapine maleate-loaded nanostructured lipid carriers: optimization and in vitro, ex vivo and in vivo evaluations. Nanomedicine (Lond.). 14(7), 889-910.

Miller, H., Zhang, J., KuoLee, R., Patel, G.B., Chen, W., 2007. Intestinal M cells: The fallible sentinels?. World J. Gastroenterol. 13, 1477-1486.

Nair, A., B., Jacob, S., A., 2016. Simple practice guide for dose conversion between animals and human. J. Basic Clin. Pharma. 7, 27-31.

Nakamura, K., Yamashita, K., Itoh, Y., Yoshino, K., Nozawa, S., Kasukawa, H., 2012. Comparative studies of polyethylene glycol-modified liposomes prepared using different PEG-modification methods. Biochim. Biophys. Acta 1818, 2801-2807.

Patel MH, Mundada VP, Sawant KK. Novel drug delivery approach via Self-microemulsifying drug delivery system for enhancing oral bioavailability of asenapine maleate: Optimization, characterization, cell uptake, and in vivo pharmacokinetic studies. AAPS PharmSciTech, 2019b, 20, 44: 1-8

Patel, M., Mundada, V., Sawant, K., 2019a. Enhanced intestinal absorption of asenapine maleate by fabricating solid lipid nanoparticles using TPGS: elucidation of transport mechanism,

permeability across Caco-2 cell line and in vivo pharmacokinetic studies. Artif Cells Nanomed Biotechnol. 47(1), 144-153.

Ribeiro LNM, Couto VM, Fraceto LF, de Paula E. Use of nanoparticle concentration as a tool to understand the structural properties of colloids, Scientific Reports. 8 (1), 2018: 982

Shete, H., Patravale, V., 2013. Long chain lipid based tamoxifen NLC. Part I: Preformulation studies, formulation development and physicochemical characterization. Int. J. Pharm. 454, 573-583.

Shreya AB, Managuli RS, Menon J, Kondapalli L, Hegde AR, Avadhani K, Shetty PK, Amirthalingam M, Kalthur G, Mutalik S. Nano-transfersomal formulations for transdermal delivery of asenapine maleate: in vitro and in vivo performance evaluations. J Liposome Res. 2016, 26 (3): 221-32.

Shreya, A.B., Raut, S.Y., Managuli, R.S., Udupa, N., Mutalik, S. 2019. Active targeting of drugs and bioactive molecules via oral administration by ligand-conjugated lipidic nanocarriers: Recent advances. AAPS PharmSciTech. 20(1), 15.

Singh SK, Hidau MK, Gautam S, Gupta K, Singh KP, Singh SK, Singh S. Glycol chitosan functionalized asenapine nanostructured lipid carriers for targeted brain delivery: Pharmacokinetic and teratogenic assessment. Int J Biol Macromol. 2018, 108:1092-1100.

Singh, S.K., Dadhania, P., Vuddanda, P.R., Jain, A., Velaga, S., Singh, S., 2016. Intranasal delivery of asenapine loaded nanostructured lipid carriers: formulation, characterization, pharmacokinetic and behavioural assessment. RSC Adv 6, 2032-2045.

Stewart, J.C.M., 1980. Colorimetric determination of phospholipids with ammonium ferrothiocyanate. Anal. Biochem. 104, 10-14.

Yun, Y., Cho, Y.W., Park, K., 2013. Nanoparticles for oral delivery: Targeted nanoparticles with peptidic ligands for oral protein delivery. Adv. Drug Deliv. Rev. 65, 822-832.

Zheng T, Bott S, Huo Q. Techniques for accurate sizing of gold nanoparticles using Dynamic Light Scattering with particular application to chemical and biological sensing based on aggregate formation. ACS Appl. Mater. Interfaces, 2016, 8: 21585−21594